POLITECNICO
MILANO 1863

SCUOLA DI INGEGNERIA INDUSTRIALE
E DELL'INFORMAZIONE

Executive Summary of the Thesis

Adjoint Shape Optimization: Cavitation Reduction for Hydrofoils

Laurea Magistrale in Aeronautical Engineering - Ingegneria Aeronautica

Author: Maddalena Rossi

Advisor: Full Prof. Alberto Guardone

Co-advisor: Phd Student Luca Abergo

Academic year: 2022-2023

1. Introduction

Sailboat foils are an innovative technology that is revolutionizing the sailing world. Foils are hydrodynamic appendages that are mounted under the boat's hull and allow it to be lifted out of the water, reducing friction and increasing speed. Sailboat foils represent a real quantum leap in sailing and are set to change the way we think about this sport and about recreational sailing. Since the hull is lifted out of the water, the submerged surface in the water, i.e. that of the foils, is much smaller. Wave resistance in the flight phase no longer exists, so the shape of the submerged appendages becomes more important (from the original concept [9], to the new contribution [17],[19]). These aerodynamic lifting surfaces are highly sensitive to geometric modifications and even slight changes in the shape can have a significant influence on the final design's performance.

In the context of designing foils for sailboats, the phenomenon of cavitation that can occur on the surface of the appendages, due to high sailing speeds, must be taken into account. Cavitation is a physical phenomenon that occurs when the pressure of a fluid reaches or drops below its vapor pressure, leading to the formation of vapor bubbles within the fluid. Avoiding cavitation is crucial, since it will have a detrimental effect on the hydrodynamic performance of the foil. Such physical phenomenon is present in many engineering systems, such as pumps, marine propellers, hydroelectric turbines and pipelines, and can cause structural damage and efficiency losses (e.g. [6] and [4]). In recent decades, cavitation research has been the subject of increasing scientific and technological interest due to its implications in many industrial applications. Indeed, understanding the dynamics of cavitation bubbles and their interactions with surrounding fluids is essential for improving the energy efficiency of systems and preventing damage to structures.

Cavitation is indeed an important concern for the hydrofoil performance, such as [15], but its numerical prediction remains a difficult problem, [7], [3], [5], [1]. These difficulties explain the reason why cavitation aspects are usually not considered in hydrofoil shape optimization, unless when the objective is precisely to delay the cavitation, such as in [20]. The goal of this thesis is not to simulate the cavitation phenomenon, but rather to search for an optimized shape to prevent its occurrence. Usually, optimization to avoid cavitation is performed using the inverse design method. This method works by prescribing the desired pressure distri-

bution, based on which the profile deformation is obtained. The disadvantage of this method is that it is not trivial to determine the pressure distribution to impose, especially in the three-dimensional case. Instead, in this thesis, the use of adjoint shape optimization is proposed to obtain a profile where the potential cavitation area is minimized. The advantage of adjoint shape optimization is that there is no need to know the pressure distribution beforehand. Usually, optimization to avoid cavitation is performed using the inverse design method. This method works by prescribing the desired pressure distribution, based on which the profile deformation is obtained. The disadvantage of this method is that it is not trivial to determine the pressure distribution to impose, especially in the three-dimensional case [10]. Instead, in this thesis, the use of adjoint shape optimization is proposed to obtain a profile where the potential cavitation area is minimized. The advantage of adjoint shape optimization is that there is no need to know the pressure distribution beforehand. The research project aims to optimize the profile shape of both a 2D and a 3D foil, with the objective of minimizing cavitation. To accomplish this, in this thesis we worked inside the optimization chain implemented in the open source finite volume solver SU2, Stanford University Unstructured software [12]. In particular, to investigate this issue, a new objective function has been coded to estimate an area of possible cavitation. This research contributes to the existing body of knowledge in hydrofoil design, exploiting a high fidelity optimization method [2] and provide novel insights into the potential of adjoint methods in tackling cavitation-related challenges.

2. Methodology

In this work, the discrete adjoint formulation is implemented using automatic differentiation (AD) to simplify the process. AD was developed based on the understanding that any simulation code, no matter how complex, can be broken down into a series of basic operations with well-known differentiation rules. By applying the chain rule iteratively within the computer program, it becomes possible to compute both the simulation output and its derivative with respect to specific design variables simultaneously.

SU2 is a tool for solving partial differential equations, multiphysics analysis, and pde-constrained optimization problems on structured and unstructured grids. The software includes a RANS iterative solver for simulating compressible, turbulent flows commonly found in problems in aerospace engineering. A number of convective fluxes discretization schemes have been implemented, such as the Jameson-Schimdt-Turkel (JST) scheme [18] and the upwind Roe scheme [13]. The turbulence can be either modeled by the Spalart-Allmaras(S-A) model [16] or the Menter Shear Stress Transport (SST) Model [8]. The discretization of Navier-Stokes equations is performed using the Finite-volume method on a vertex-based median-dual grid, with several numerical schemes to solve the convective fluxes implemented. The software can also be used for multi-physics problems, including fluid-structure interaction problems and acoustics, as well as for automatic shape optimization. The surface sensitivity is computed using the discrete adjoint and projected into the design space, with the body described using the Free Form Deformation (FFD) method [14]. The mesh around the body is updated, and the optimization algorithm used is gradient-based. One notable advantage of AD, thanks to its construction, is that it avoids introducing truncation errors typically associated with traditional finite difference methods. In other words, the derivatives calculated using AD are accurate up to the precision of the machine, without any loss of accuracy.

2.1. Cavitation Objective Function

Cavitation is the physical phenomenon according to which the pressure of water decreases until it equals or exceeds the vapor pressure under given conditions of pressure and temperature. Cavitation leads to the formation of air bubbles on the surface of the profile, which strongly impacts the aerodynamic performance of the profile. They can also affect the properties of the material from which the surface is made. The work reporting this thesis is the implementation of a part of SU2 code that checks for cavitation on a profile and optimizes the shape of the profile with the goal of nullifying this damaging phenomenon. The implemented code works by calculating for each grid element the difference

between pressure and vapor pressure, in dimensionless terms. In case the following inequality occurs:

$$-C_p - \sigma > 0 \tag{1}$$

the code computes the cavitation coefficient:

$$Coeff_{Cav} = \frac{\sum_{i=1}^{n} A_i | - C_{pi} - \sigma |}{A_{ref}} \tag{2}$$

where σ is the cavitation number in the simulating condition, C_{pi} is the pressure value in the i-th element, A_i is the area of the i-th element, A_{ref} is the reference area chosen to dimensionalize. Then the cavitation coefficient is given by the summation of the product of the pressure difference by the area of the element, for each element in which cavitation occurs (i.e., the inequality given above is true). This is made dimensionless by dividing by a reference area chosen by the user and given in the configuration file. In the case of 2D analysis, the quantity used for adimensionalization is not an area, but rather a length. It is also possible to derive the total cavitation area by summing the areas of the elements in which the phenomenon is evidenced:

$$A_{Cav} = \sum_{i=1}^{n} A_i \tag{3}$$

The cavitation number, σ, is defined by the user within the configuration file. When a simulation is launched, the code is able to print the cavitation coefficient values in the history file. In the case of shape optimization, the cavitation coefficient itself can be defined as an objective function. Infact it is possible to choose as objective function either the cavitation coefficient either the cavitation area, to be reduced.
The cavitation number is obtained by the following formula:

$$\sigma = \frac{P_{ref} - P_{vap}}{\frac{1}{2}\rho_{ref} \cdot v_{ref}^2} \tag{4}$$

substituting the values of the quantities characteristic of the case being studied. In the equation above, P_{ref} represents the reference pressure at which the simulation is conducted, ρ_{ref} denotes the reference density, and v_{ref} corresponds to the reference velocity. The values employed for these quantities in the simulations of this project are listed in the 2D results section.

The cavitation number provides a measure of the relative difference between the local pressure and the vapor pressure of the fluid. When the cavitation number is close to or exceeds unity ($\sigma \geq 1$), cavitation is likely to occur. Conversely, when the cavitation number is significantly below unity ($\sigma \ll 1$), cavitation effects are minimal.
The typical values of the cavitation number for profiles can vary depending on the specific application and operating conditions. In general, for hydrofoils, propellers, and other underwater profiles, typical cavitation numbers range from 0.2 to 2.0. These profiles experience varying degrees of cavitation depending on factors such as the flow velocity, pressure distribution, and geometry.
For aircraft wings, which operate in air rather than water, the cavitation numbers are typically much lower. The cavitation number for airfoils can be in the range of 10^{-4} to 10^{-2} or even lower. This is due to the higher vapor pressure of air compared to water, making cavitation effects less prevalent in aerodynamic applications.

3. Verification

The research focuses on finding the optimal shape using gradient-based algorithms. To achieve this, it is necessary to determine the sensitivity of the objective function with respect to the design variables. Generally, the objective function J can be comprised of n_f individual functions denoted as J_k, each of which must be defined and differentiated with respect to the design parameters. The relationship between the objective functions, and the mesh can be clarified by the following expression:

$$J_k(\alpha) = J_k(U(\alpha), X(\alpha)) \quad \text{for } k \in \{1, \ldots, n_f\} \tag{5}$$

Initially, the objective was to calculate the partial derivatives $\frac{\partial J_k(\alpha)}{\partial \alpha_i}$, which would involve $n_f \times n_\alpha$ derivatives. However, more recent codes calculate the total derivative $\frac{dJ_k}{dX}$ for k $\in \{1...n_f\}$. These codes incorporate both the direct influence of node positions and the indirect influence caused by changes in the flow field to achieve steady-state convergence. The Finite Difference method is a straightforward and traditional approach for obtaining the gradient of the objective function. This method does not require any

modifications to the solver. To calculate the object function gradient, the discrete flow solution needs to be computed for the given foil described by the design variables α, as well as for perturbed values $(\alpha+\delta\alpha)$ and $(\alpha-\delta\alpha)$. Typically, a second-order finite difference scheme is employed.
If the geometry of the body is defined using an FFD box, as in this work, a perturbation in the direction m of a quantity $\delta\alpha$ is represented by shifting a designated vertex, which serves as a design variable. This leads to two mesh deformations, $X(\alpha + \delta\alpha_m)$ and $X(\alpha - \delta\alpha_m)$, that need to be performed, and two flow solutions are computed on the morphed grids, satisfying the following conditions:

$$R(U(\alpha - \delta\alpha), X(\alpha - \delta\alpha)) = 0 \quad (6)$$
$$R(U(\alpha + \delta\alpha), X(\alpha + \delta\alpha)) = 0 \quad (7)$$

However, this method becomes impractical when dealing with a large number of design variables because computing the matrix $\frac{dJ_\alpha}{d\alpha}$ incurs a cost equivalent to $2 \times n_\alpha$ times the cost of a single flow solution. The verification of the adjoint solver is performed by comparing the obtained gradients with a second-order centered finite difference method:

$$f'(x) = \frac{f(x+h) - f(x-h)}{2h} \quad (8)$$

where h represents the step size. One critical aspect to consider is how to determine the appropriate step size. The choice of step size significantly impacts the accuracy of the computed gradient. If the step size is too small, rounding errors become significant. Conversely, if it is too large, the truncation of higher-order terms in the Taylor expansion is no longer valid.
In the current study the verification is carried out considering the NACA 0015. The surface is parameterized using a two-dimensional FFD box, with 14 design variables. The box containing the profile and the DVs are riported in Figure 1, where it is also shown the direction of the possible displacements. The shape can be modified changing the thickness and camber of the airfoil.Before reaching this size of the box, other dimensions were tested, starting from larger sizes and gradually reducing the box, so that the edges were much closer to the profile. A reasonable value for the step size for finite differences was found to be 10^{-5}. Very good agreement is found between the sensitivities calculated with finite differences and with the discrete adjoint method. A direct comparison between the two methods is observable in Figure2, where the cavitation sensitivity is plotted with respect to the design variables.

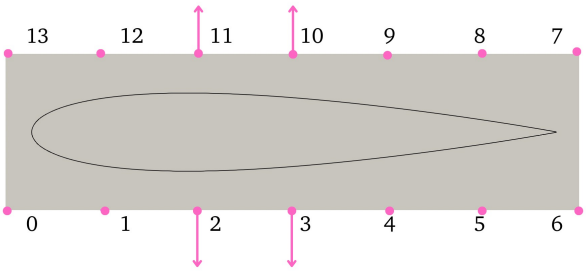

Figure 1: 2D box and design variables

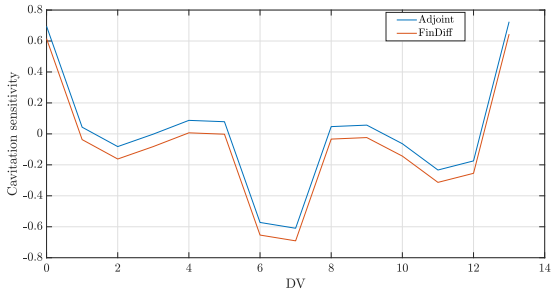

Figure 2: Cavitation sensitivity computed with the adjoint method and with the finite difference

4. Results

This section presents the results of the cavitation optimization, which is divided into two parts: the first part focuses on the 2D case using the NACA 0015 airfoil, while the second part discusses the 3D Moth foil.

4.1. NACA 0015 Optimization

Starting with the two-dimensional profile, the chosen free stream conditions are provided in Table 1. The target of the optimization is to reduce the possible area of cavitation. The optimizations are carried out with a fixed value of C_l, which was determined through prior direct simulations. The angle of attack is let free to vary in order to more easily respect the constraint about the lift.

The free stream velocity was chosen to be equal to that in the paper [11], as mentioned above. The density and dynamic viscosity are typical values for water. The Reynolds number was calculated considering the chord length of the profile, which is equal to 1 m, as the reference length.

Velocity	$8\ m/s$
Temperature	20°C
Density	$998.2\ kg/m^3$
Viscosity	$8.9 \times 10^{-4} kg/(m \cdot s)$
Reynolds	8.97×10^6
C_l **constraint**	0.876

Table 1: Free stream conditions

Given the boundary conditions mentioned above, the cavitation number σ is found to be 1.937. This value is obtained using Equation 4, knowing that the reference pressure is computed as $P_{ref} = \rho_{ref} v_{ref}^2 = 63884.8Pa$. Considering the water temperature to be 20°C, the vapor pressure value $P_{vap} = 2000Pa$ is extracted from the tabulated data. By comparing the value of σ with the pressure coefficient visualization in Figure 7, it confirms the presence of cavitation on the upper surface of the profile, specifically in the leading edge region. Here, the magnitude of the pressure coefficient is greater than the cavitation number. The same result is visible in Figure 6, which depicts the cavitation area A_{Cav} before optimization. The cavitation area includes elements on the profile that satisfy the inequality stated in Equation 1.
The body is parameterized with a single FFD box and has 14 design variables that can be moved in the y direction (see Figure 1). The mesh deformation in this two dimensional study follows the linear elastic equation ELA. The history of optimization is reported in Figure 3. It can be noticed that, after 9 design loops, cavitation decreases to zero. Additionally, the trend of the cavitation area is also shown in the same graph, demonstrating a clear decrease. The cavitation area is expressed as a percentage relative to a reference area A_{ref}. The chosen reference area has a value of unity.

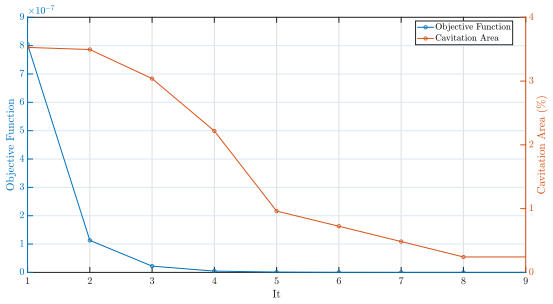

Figure 3: Objective function and cavitational area wrt design loops

Figure 4 depicts the evolution of the airfoil shape after 9 design loops of optimization. The obtained profile is asymmetric, with a downward-leading edge and an upward-trailing edge. The modification of the leading edge is a characteristic feature of profiles aimed at increasing the pressure ahead of the flow. The increase in curvature on the leading edge generates a lower peak in the pressure coefficient. The last part of the profile is deflected upright, to compensate for the change in the leading edge, as well as to satisfy the constraint on the lift. Graph 5 compares the pressure coefficient distribution of the NACA 0015 airfoil with that of the optimized airfoil. It highlights that the magnitude of the pressure coefficient decreases in the leading-edge region, eventually becoming lower than the cavitation number.
This result is further confirmed by the comparison of Figures 7 and 8. The first image represents the NACA 0015 profile, while the second image represents the optimized profile. We can observe that the peak value of the coefficient of pressure (C_p) has decreased, and simultaneously, the area of minimum C_p along the profile's upper surface has increased. In the given operating conditions, the previously existing cavitation area on the NACA 0015 profile has now been completely eliminated through shape modification. This remarkable achievement signifies that the air bubble, which used to occupy the dark blue-colored region along the profile, has been effectively flattened due to the optimized profile shape.

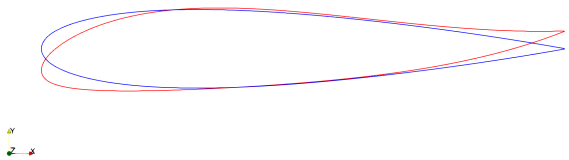

Figure 4: Comparison between NACA0015 (blu) and the optimized profile (red)

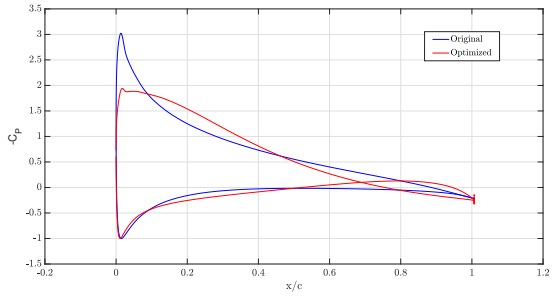

Figure 5: Pressure coefficient of NACA0015 and the optimized profile

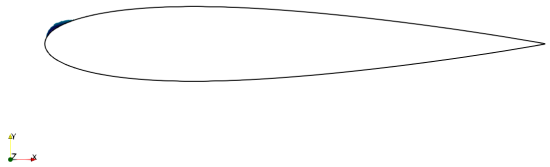

Figure 6: Cavitation area on NACA0015

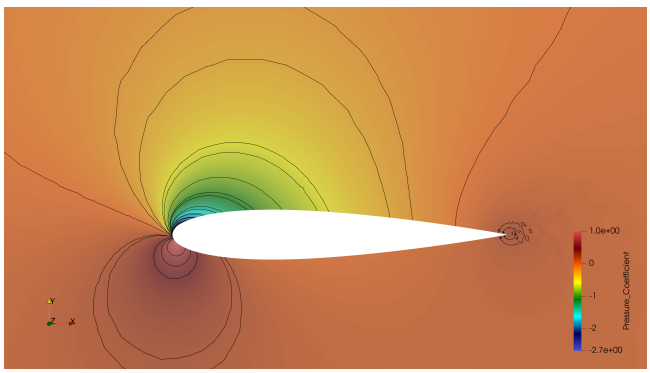

Figure 7: Pressure contours on the NACA 0015

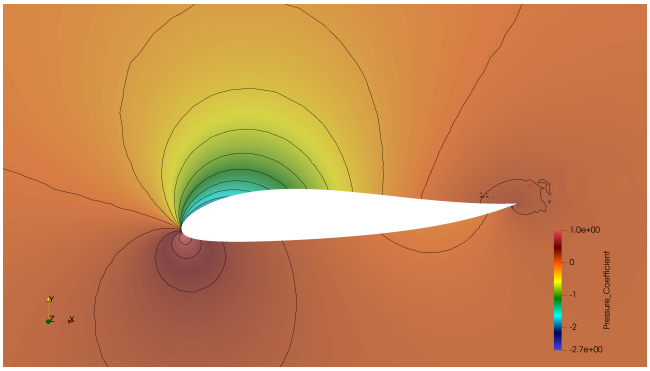

Figure 8: Pressure contours on the optimized profile

It can be noticed that the reduction in cavitation area generates an increase of drag. This can be expected since the two sensitivities are different and have different local minima. Actually, we are not able to simulate cavitation, so if we had a cavitation model, the actual drag would likely be higher. Therefore, reducing cavitation could also mean reducing drag. It cannot be concluded that reducing cavitation automatically leads to an increase in drag, but it may depend on the specific case and further studies are needed. For example, in the next section, it will be shown that the drag has not increased.
Leaving the angle of attack unconstrained aids in the optimization process, but there is a significant modification of 5 in the angle of attack, which is a substantial change. In the future, the optimization could be repeated while keeping the angle of attack fixed, for example.

	1 loop	9 loop
Cavitation Area	3.52788%	0.24247%
AoA	7.25413°	12.3547°
C_d	0.011729	0.012295

Table 2: 2D results

The elimination of the cavitation area is of significant importance as it indicates a successful mitigation of the detrimental effects caused by cavitation. The modified profile shape encourages smoother flow behavior and reduces the occurrence of low-pressure regions that could trigger cavitation. Consequently, the negative effects associated with the presence of cavitation, such as performance degradation and potential

damage, are effectively eliminated.
The successful elimination of the cavitation area demonstrates the effectiveness and potential of the adjoint shape optimization method in addressing cavitation-related challenges.

4.2. Hydrofoil Optimization

Regarding the 3D case, the main foil of the Moth sailboat designed by the PoliMi Sailing Team was optimized. The target of optimization is the cavitation area, keeping constant the lift of the baseline geometry. The main foil is equipped with a central bulb, which serves as the junction point with the vertical surface. In the analyzed case, only half of the foil was considered, taking advantage of its symmetry to reduce computational time.
The foil was encapsulated within a free-form deformation box, as shown below in Figure 9. The vertices highlighted in black represent the control points with freedom of displacement in the z-direction. The DVs are 126, 7 in the chord direction, 9 in the span direction. Since the design variables are only allowed to move along the z-axis, neither the chord length nor the span length can change. The bulb is not part of the optimization. First-order continuity properties are applied at the intersection.
Similar to the 2D case, the boundary conditions used for this optimization were applied, as the Moth sailboat is assumed to operate at a speed of approximately 15 knots in lake waters during the summer. As a result, the cavitation number remains unchanged at 1.937. Only the fixed value of C_l is different, in this case equal to 1.41.
The grid surrounding the foil was created using Pointwise and is an unstructured grid in the shape of a hemisphere. The region around the wing was structured using the T-Rex mode in 3D.
RANS equations are solved with SA turbulence model, JST is used to calculate the fluxes. 2^{nd} and 4^{th} order artificial dissipation coefficients are 0.5 and 0.02. It is required to have at least six order reduction of the relevant residuals and the finals lower than $10^{(-13)}$.
As mesh deformation method in this optimization test case RBF has been used. RBF has been settlend using Wendland C2 as baseline functions are selected, using a number of control points equal to 15% of total number of surface elements.

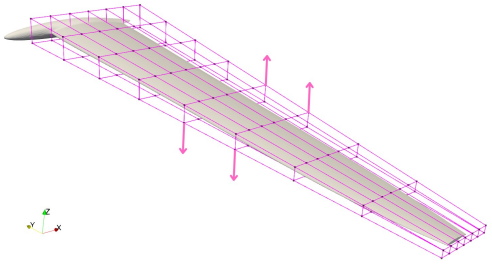

Figure 9: 3D box

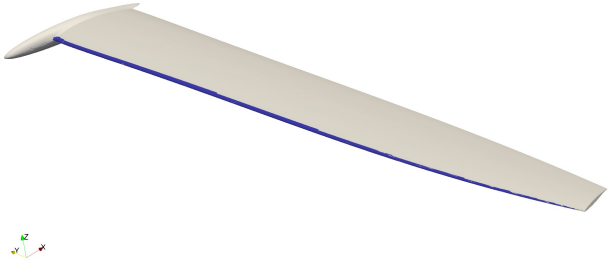

Figure 10: Cavitational area in the original foil

In Figure 10, the surface area affected by cavitation is highlighted. It was visualized by examining the pressure coefficient, using a threshold value of $\sigma = 1.937$. The reference area used to compute the A_{Cav} corresponds to 0.0287 m^2.
Due to limited computational resources, only 5 design loops were completed. The optimality conditions are not fullfilled, but we are stuck in a local minimum. We can consider the obtained shape as optimized since the cavitation coefficient is reduced of the 3%. As can be seen from Table 3, a decrease in cavitation area suggests that the modifications made to the profile have effectively mitigated the detrimental effects of cavitation.
In this three-dimensional case, an improvement in fluid dynamics performance was also achieved, as the drag coefficient decreased from the first to the fifth design loop. The decrease in the drag coefficient observed during the cavitation optimization process is a positive outcome, despite not being the objective of the optimization. In this case, it can be observed that the angle of

attack has changed much less compared to the 2D case.

	1 loop	5 loop
Cavitation Area	7.11743%	4.58159%
AoA	7.91938°	9.76929°
C_d	0.052297	0.051707

Table 3: Design loops

Figure 11 compares the original foil with the optimized foil, displaying their respective cavitation areas. The original foil is colored yellow, and its cavitation area is depicted in blue, extending throughout the foil's span, particularly at the leading edge. In contrast, the optimized foil is colored aqua green, and its cavitation area is barely noticeable. A small red area is observed near the junction with the bulb.
For further clarity, the pressure coefficient distributions are shown from a top view, along with pressure distribution isolines (Figures 12, 13). It is noticeable that in the optimized foil the region with the lowest C_p is narrower compared to the original case and close to the interface with the bulb. However, this is nearby the area that is not optimized. This suggests the possibility of optimizing the junction region between the bulb and the foil in the future.
The residual presence of cavitation is due to the premature termination of the optimization; otherwise, it would have decreased further.

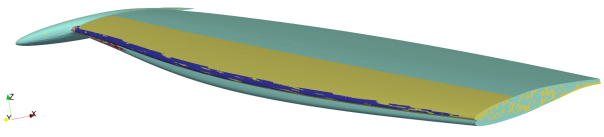

Figure 11: Cavitational area in the original foil and optimized foil

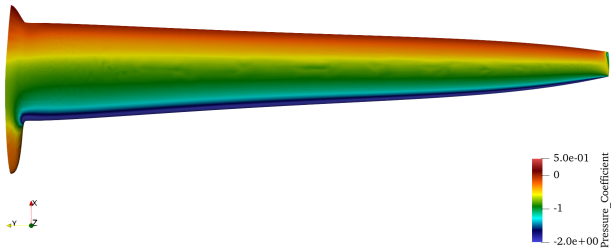

Figure 12: Pressure coefficient of the original foil

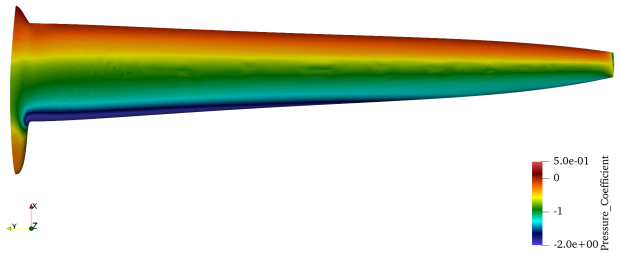

Figure 13: Pressure coefficient of the optimized foil

5. Conclusions

This thesis is focused on the application of adjoint shape optimization techniques for reducing cavitation on hydrofoils. Indeed, usually in this field, the inverse design method had been predominantly used to search for the optimal shape that avoids cavitation. The use of adjoint shape optimization offers the advantage of not requiring prior knowledge of the pressure distribution, unlike inverse design. The objective of this research project was to optimize the profile shape of a 2D and a 3D foil, with the goal of minimizing cavitation. To achieve this, the optimization framework implemented in the open-source finite volume solver SU2 was exploited. In order to address this objective, a new objective function was developed to estimate the potential cavitation area.
A successful result has been achieved in both the two-dimensional and three-dimensional studies. By utilizing sensitivity information obtained from the adjoint solver, it was possible to systematically modify the hydrofoil's shape to mitigate cavitation-related issues. In the 2D case,

a profile with virtually no cavitation area was achieved, accompanied by a significant change in the angle of attack. In the 3D case, after only 5 design iterations, a reduction in the cavitation area was observed, resulting in a decrease in the drag coefficient as a side effect. In this case, the variation in the angle of attack was only 2°. The 3D hydrofoil studied in this case is the main foil dseigned and produced for a Moth by the PoliMi Sailing Team. The successful elimination of the cavitation area demonstrates the effectiveness and potential of the adjoint shape optimization method in addressing cavitation-related challenges.
It should be noted that the optimal solution highly depends on the specific design requirements and operating conditions. The choice of design variables, objective functions, and constraints must be carefully tailored to the hydrofoil's intended application and operational environment. Future studies can explore additional design variables and multi-objective optimizations to achieve a more comprehensive and robust hydrofoil design. Overall, the successful implementation of adjoint shape optimization for cavitation reduction presents a promising avenue for further research and potential real-world applications. In the future, for instance, the optimization could be repeated while keeping the angle of attack fixed. It is hoped that the outcomes of this study will contribute to the advancement of hydrofoil design and optimization techniques, ultimately benefiting the efficiency, sustainability, and performance of hydrofoil-based systems in various industries.

6. Bibliography

References

[1] Deniz Tolga Akcabay, Eun Jung Chae, Yin Lu Young, Antoine Ducoin, and Jacques Andre Astolfi. Cavity induced vibration of flexible hydrofoils. *Journal of Fluids and Structures*, 49:463–484, aug 2014.

[2] Dimitra Anevlavi and Kostas Belibassakis. An adjoint optimization prediction method for partially cavitating hydrofoils. *Journal of Marine Science and Engineering*, 9(9):976, sep 2021.

[3] Olivier Coutier-Delgosha, François Deniset, Jacques André Astolfi, and Jean-Baptiste Leroux. Numerical prediction of cavitating flow on a two-dimensional symmetrical hydrofoil and comparison to experiments. *Journal of Fluids Engineering*, 129(3):279–292, aug 2006.

[4] H. Ding, F. C. Visser, Y. Jiang, and M. Furmanczyk. Demonstration and validation of a 3d CFD simulation tool predicting pump performance and cavitation for industrial applications. *Journal of Fluids Engineering*, 133(1), jan 2011.

[5] Antoine Ducoin, François Deniset, Jacques André Astolfi, and Jean-François Sigrist. Numerical and experimental investigation of hydrodynamic characteristics of deformable hydrofoils. *Journal of Ship Research*, 53(04):214–226, dec 2009.

[6] Parag R. Gogate and Abhijeet M. Kabadi. A review of applications of cavitation in biochemical engineering/biotechnology. *Biochemical Engineering Journal*, 44(1):60–72, apr 2009.

[7] Jean-Baptiste Leroux, Olivier Coutier-Delgosha, and Jacques André Astolfi. A joint experimental and numerical study of mechanisms associated to instability of partial cavitation on two-dimensional hydrofoil. *Physics of Fluids*, 17(5):052101, may 2005.

[8] F. Menter. Zonal two equation kw turbulence models for aerodynamic flows. *23rd fluid dynamics,plasmadynamics, and lasers conference*, 1993.

[9] John Henry Michell. The wave resistance of a ship. *Phil.Mag*, 5(45):106–123, 1898.

[10] Jeremy Nahon, Mehrdad Zangeneh, Motohiko Nohmi, Hiroyoshi Watanabe, and Akira Goto. A robust inverse design solver for controlling the potential aggressiveness of cavitating flow on hydrofoil cascades. *International Journal for Numerical Methods in Fluids*, 93(7):2291–2310, apr 2021.

[11] Motohiko Nohmi, Tomoki Tsuneda, Byungjin An, and Takayuki Suzuki. Cavitation CFD prediction for NACA0015

hydrofoil flow considering boundary layer characteristics. pages 185–190, 2018.

[12] Francisco Palacios, Juan Alonso, Karthikeyan Duraisamy, Michael Colonno, Jason Hicken, Aniket Aranake, Alejandro Campos, Sean Copeland, Thomas Economon, Amrita Lonkar, Trent Lukaczyk, and Thomas Taylor. Stanford university unstructured : An open-source integrated computational environment for multi-physics simulation and design. jan 2013.

[13] P.L. Roe. Approximate riemann solvers, parameter vectors, and difference schemes. *Journalof computational physics*, page pp. 357–372, 1981.

[14] Jamshid Samareh. Aerodynamic shape optimization based on free-form deformation. aug 2004.

[15] M. Sedlar, B. Ji, T. Kratky, T. Rebok, and R. Huzlik. Numerical and experimental investigation of three-dimensional cavitating flow around the straight NACA2412 hydrofoil. *Ocean Engineering*, 123:357–382, sep 2016.

[16] P. Spalart and S. Allmaras. A one-equation turbulence model for aerodynamic flows. jan 1992.

[17] L.N. Sretenskii. *Theory of wave motions in a fluid*. Moscow Izdatel Nauka, 1977.

[18] R.C Swanson and Eli Turkel. On central-difference and upwind schemes. *Journal of Computational Physics*, 101(2):292–306, aug 1992.

[19] Marcos de Parahyba Campos Tsugukiyo Hirayama. New experimental trials for obtaining the added wave resistance f sailing yacht in heeled and yawed condition. *J. Kansai Soc. N. A.*, 1998.

[20] Qun Wei, Hong xun Chen, and Rui Zhang. Numerical research on the performances of slot hydrofoil. *Journal of Hydrodynamics*, 27(1):105–111, feb 2015.